A nonlinear viscoelastic model for NSGT nanotubes conveying fluid incorporating slip boundary conditions

Ali Farajpour [a*], Hamed Farokhi [b], Mergen H. Ghayesh [a]

[a] *School of Mechanical Engineering, University of Adelaide, South Australia 5005, Australia*

[*] *Corresponding author's email: ali.farajpourouderji@adelaide.edu.au (A. Farajpour)*
Email: mergen.ghayesh@adelaide.edu.au (M.H. Ghayesh)

[b] *Department of Mechanical and Construction Engineering, Northumbria University, Newcastle upon Tyne NE1 8ST, UK*
Email: hamed.farokhi@northumbria.ac.uk (H. Farokhi)

Abstract

A nonlinear viscoelastic model is developed for the dynamics of nanotubes conveying fluid. The influences of strain gradients and stress nonlocality are incorporated via a nonlocal strain gradient theory (NSGT). Since at nanoscales, the assumptions of no-slip boundary conditions are not valid, the Beskok-Karniadakis theory is used to overcome this problem. The coupled nonlinear differential equations are derived via performing an energy/work balance. The derived equations along the transverse and axial axes are simultaneously solved to obtain the nonlinear frequency response. For this purpose, Galerkin's technique together with a continuation method are utilised. The frequency response is investigated in both subcritical and supercritical flow regimes.

Keywords: Nanoscale tubes; Fluid velocity; Viscoelasticity; Coupled motion; Scale effects

1. Introduction

Nanoscale structures conveying fluid have many interesting applications in different nanomechanical systems such as nanoscale sensors, nanosystems for tumour targeting and nanodevices for the early diagnosis of serious diseases. Understanding the interactions between the fluid and fundamental structure is important in these nanosystems, especially when there are large external forces.

Fluid-conveying nanoscale structures can have a large number of molecules, which make molecular dynamics simulations computationally costly and time-consuming. On the other hand, since these systems have very small dimensions, it is formidable to experimentally analyse the mechanical response. As a result, a considerable amount of attention has been directed toward the continuum-based modelling of fluid-conveying micro/nanoscale structures (Atashafrooz et al., 2018; Mohammadimehr et al., 2017; Hosseini et al., 2018; Kural and Özkaya, 2017). Classical continuum mechanics can reasonably describe the mechanics of macroscale structures (Ghayesh and Moradian, 2011; Kazemirad et al., 2013; Farokhi et al., 2018). However, from physical point of view, the classical continuum mechanics is not reasonable as it is not able to describe size influences (Farajpour et al., 2018a; Aydogdu, 2015; Arda and Aydogdu, 2018; Gholipour et al., 2015; Farokhi and Ghayesh, 2015). To overcome this problem, a few size-dependent theories involving the couple stress model (Akgöz and Civalek, 2012; Park and Gao, 2006; Ghayesh et al., 2013; Farokhi and Ghayesh, 2018; Nejad et al., 2017; Farokhi and Ghayesh, 2017), pure nonlocal elasticity (PNE) (Malekzadeh and Shojaee, 2015; Zenkour, 2018; Farajpour et al., 2018b; Asemi and Farajpour, 2014) and nonlocal strain gradient theory (NSGT) (Li and Hu,

2015; Farajpour et al., 2019; Numanoğlu et al., 2018) have been suggested. In this study, the second one (i.e. NSGT) is used for describing size influences.

A notable amount of effort has lately been made in order to understand the mechanics of micro/nanoscale tubes conveying fluid via use of size-dependent theories of elasticity. Wang (Wang, 2010) extracted the oscillation characteristics of fluid-conveying microscale tubes; he modelled size influences on the oscillation characteristics by employing a couple stress theory. Moreover, Lee and Chang (Lee and Chang, 2008) employed the PNE in order to explore the linear oscillation of nanotubes conveying fluid incorporating transverse deflections. Soltani et al. (Soltani et al., 2010) also examined the effects of a viscoelastic foundation on the oscillation and stability of fluid-conveying nanotubes via use of a size-dependent model. In another study, Zeighampour and Beni (Zeighampour and Beni, 2014) developed a linear continuum model for a system of two nanoscale tubes conveying fluid incorporating the influences of couple stresses. In addition, thermal influence on the oscillation and stability of fluid-conveying nanotubes was examined in Ref. (Zhen et al., 2011) by employing the PNE. A continuum model incorporating size effects was also proposed by Maraghi et al. (Maraghi et al., 2013) for examining the oscillation and stability characteristics of a particular type of fluid-conveying nanotubes with piezoelectric properties. The influences of stress nonlocality as well as the effects of fluid pulsation on the instability of nanotubes were also explored by Liang and Su (Liang and Su, 2013). In another study, Askari and Esmailzadeh (Askari and Esmailzadeh, 2017) proposed a continuum model for analysing the effects of a nonlinear medium on the forced vibration response of nanoscale tubes conveying fluid; thermal effects were also taken into consideration. The nonlocal version of the Euler-Bernoulli theory was also used by Ghasemi et al. (Ghasemi et al., 2013) for capturing size effects on the nonlinear stability of a system of nanotubes

conveying fluid. Moreover, the wave propagation characteristics (Li and Hu, 2016), axial vibration (Oveissi et al., 2016), flutter instability (Bahaadini and Hosseini, 2016) of fluid-conveying nanoscale tubes have recently been studied via several size-dependent models of elasticity.

In real situations, the linear assumption, which is made in many of the above-mentioned articles, is not valid for large deformations. Although the vibration of fluid-conveying nanotubes with large deformations has been investigated in a few investigation, no nonlinear viscoelastic models have been presented for the frequency response of nanotubes conveying nanofluid incorporating both transverse deflections and axial displacements. This encourages us to analyse this problem in this paper. Both strain gradients and stress nonlocality are captured employing a NSGT model. To model the occurrence of slip in the interface between the fluid and nanotube, the Beskok-Karniadakis theory is used. The Kelvin-Voigt model is also employed for describing the effects of viscoelastic properties on the nonlinear frequency response. To derive the coupled equations of motions, an energy/work balance is performed according to Hamilton's principle. A numerical solution is presented via application of Galerkin's technique and a continuation scheme. The present results could be useful for the fabrication of nanomechanical devices using fluid-conveying nanotubes.

2. A NSGT-based modelling

Figure 1 illustrates a viscoelastic nanoscale tube conveying fluid subject to an externally applied load; the tube length and outer diameter are indicated by L and d_o,

respectively; moreover, the velocity of the fluid is indicated by *U*. Utilising the Euler–Bernoulli model of beams, the strain is (Reddy, 2010)

$$\varepsilon_{xx} = -z\frac{\partial^2 w}{\partial x^2} + \frac{1}{2}\left(\frac{\partial w}{\partial x}\right)^2 + \frac{\partial u}{\partial x}. \tag{1}$$

Here *w* and *u* stand for the centre-line transverse and axial displacements, respectively. In the present NSGT-based modelling, the stress resultants are given by

$$\begin{Bmatrix} N_{xx(t)} \\ M_{xx(t)} \end{Bmatrix} = \int_A \begin{Bmatrix} t_{xx(t)} \\ z t_{xx(t)} \end{Bmatrix} dA, \tag{2}$$

where $t_{xx(t)}$ and *A* are the total stress and cross-sectional area. The NSGT-based constitutive relation is (Ghayesh and Farajpour, 2018a)

$$\begin{aligned} \Gamma_n t_{xx(t)} &= E\Gamma_g\left(\frac{\partial u}{\partial x} + \frac{1}{2}\left(\frac{\partial w}{\partial x}\right)^2\right) - zE\Gamma_g\frac{\partial^2 w}{\partial x^2} \\ &+\eta\Gamma_g\left(\frac{\partial^2 u}{\partial t\partial x} + \frac{\partial w}{\partial x}\frac{\partial^2 w}{\partial x\partial t}\right) - z\eta\Gamma_g\frac{\partial^3 w}{\partial x^2\partial t}, \end{aligned} \tag{3}$$

where

$$\Gamma_n(\bullet) = (\bullet) - (e_0 l_n)^2\nabla^2(\bullet), \tag{4}$$

$$\Gamma_g(\bullet) = (\bullet) - l_g^2\nabla^2(\bullet), \tag{5}$$

where Γ_g and Γ_n stand for the strain gradient and nonlocal operators, respectively; ∇^2, l_g, e_0, η, l_n and *E* represent the Laplacian operator, strain gradient parameter, a coefficient for calibrating the model, viscosity coefficient, internal characteristics length and Young's modulus, respectively (Ghayesh and Farajpour, 2018b). In general, the nonlocal and strain gradient parameters are obtained from experimental data or the results of molecular dynamics (MD). In the literature, MD simulations were performed to determine these scale parameters for both nanotubes and fluid-conveying nanotubes (Mohammadi et al., 2018;

Mehralian et al., 2017a; Mehralian et al., 2017b). The values of nonlocal and strain gradient parameters, which are taken in the present paper, are in the recommended range obtained by MD simulations. Employing Eqs. (2) and (3), one obtains the stress resultants as

$$\Gamma_n N_{xx(t)} = EA\Gamma_g\left(\frac{1}{2}\left(\frac{\partial w}{\partial x}\right)^2 + \frac{\partial u}{\partial x}\right) + \eta A\Gamma_g\left(\frac{\partial^2 w}{\partial t\partial x}\frac{\partial w}{\partial x} + \frac{\partial^2 u}{\partial t\partial x}\right), \tag{6}$$

$$\Gamma_n M_{xx(t)} = -EI\Gamma_g\frac{\partial^2 w}{\partial x^2} - \eta I\Gamma_g\frac{\partial^3 w}{\partial x^2\partial t}, \tag{7}$$

in which I is the nanotube moment of inertia. The energy and work associated with the elastic and viscous parts of the constitutive equation are formulated by

$$\delta U_e = \int_0^L\int_A \sigma^{(1)}_{xx(e)}\nabla\delta\varepsilon_{xx}dAdx + \int_0^L\int_A \sigma_{xx(e)}\delta\varepsilon_{xx}dAdx, \tag{8}$$

$$\delta W_v = -\int_0^L\int_A \sigma^{(1)}_{xx(v)}\nabla\delta\varepsilon_{xx}dAdx - \int_0^L\int_A \sigma_{xx(v)}\delta\varepsilon_{xx}dAdx, \tag{9}$$

where W_v and U_e denote the viscous work and elastic energy of the NSGT nanoscale tube, respectively; ∇, $\sigma^{(1)}_{ij(k)}$ and $\sigma_{ij(k)}$ represent the gradient operator, first-order and zeroth-order nonlocal stresses, respectively; "*v*" and "*e*" are used to indicate the viscoelastic and elastic parts, respectively . The stress components satisfy the following relations (Lim et al., 2015)

$$\begin{Bmatrix} t_{xx(t)} \\ t_{xx(e)} \\ t_{xx(v)} \end{Bmatrix} = \begin{Bmatrix} \sigma_{xx(t)} \\ \sigma_{xx(e)} \\ \sigma_{xx(v)} \end{Bmatrix} - \nabla\begin{Bmatrix} \sigma^{(1)}_{xx(t)} \\ \sigma^{(1)}_{xx(e)} \\ \sigma^{(1)}_{xx(v)} \end{Bmatrix} \tag{10}$$

and

$$\begin{Bmatrix} t_{xx(t)} \\ \sigma_{xx(t)} \\ \sigma^{(1)}_{xx(t)} \end{Bmatrix} = \begin{Bmatrix} t_{xx(e)} \\ \sigma_{xx(e)} \\ \sigma^{(1)}_{xx(e)} \end{Bmatrix} + \begin{Bmatrix} t_{xx(v)} \\ \sigma_{xx(v)} \\ \sigma^{(1)}_{xx(v)} \end{Bmatrix}. \tag{11}$$

For the kinetic energy of the NSGT nanoscale tube, one has

$$\delta T_k = m\int_0^L \frac{\partial w}{\partial t}\delta\frac{\partial w}{\partial t}dx + m\int_0^L \frac{\partial u}{\partial t}\delta\frac{\partial u}{\partial t}dx$$
$$+M\int_0^L \left(\kappa_{nf1}U\frac{\partial w}{\partial x}+\frac{\partial w}{\partial t}\right)\left(\kappa_{nf1}U\delta\frac{\partial w}{\partial x}+\delta\frac{\partial w}{\partial t}\right)dx \quad (12)$$
$$+M\int_0^L \left(\kappa_{nf1}U\frac{\partial u}{\partial x}+\kappa_{nf1}U+\frac{\partial u}{\partial t}\right)\left(\kappa_{nf1}U\delta\frac{\partial u}{\partial x}+\delta\frac{\partial u}{\partial t}\right)dx,$$

where *M* and *m* stand for the fluid and nanotube masses per length, respectively; κ_{nf1} indicates the velocity correction factor (Beskok and Karniadakis, 1999). The following relation is obtained for this factor by employing the Beskok-Karniadakis theory

$$\kappa_{nf1} = \lambda Kn - 4Kn\left(\frac{\lambda Kn+1}{-1+\beta Kn}\right)\left(-1+\frac{2}{\sigma_v}\right)+1, \quad (13)$$

and

$$\lambda = \frac{2\lambda_0}{\pi}\tan^{-1}\left[\lambda_1\left(Kn\right)^{\lambda_2}\right]. \quad (14)$$

Here *Kn* stands for the Knudsen number; β, σ_v and λ_i are constant coefficients, which are equal to $\beta=-1$, $\sigma_v=0.7$ and $\langle\lambda_0,\lambda_1,\lambda_2\rangle=\langle 64/(15\pi),4,0.4\rangle$, respectively. For the work done by the externally applied load, one has

$$\delta W_q = \int_0^L q_F\delta w\,\mathrm{d}x, \quad (15)$$

where

$$q_F = F(x)\cos(\omega t). \quad (16)$$

In the above equation, *F* and ω represent the loading amplitude and excitation frequency respectively. Substituting Eqs. (8), (9), (12) and (15) into Hamilton's principle described by

$$\int_{t_1}^{t_2}\left(\delta W_v-\delta U_e+\delta W_q+\delta T_k\right)\mathrm{d}t=0, \quad (17)$$

the motion equations in terms of $N_{xx(t)}$ and $M_{xx(t)}$ are derived as

$$\frac{\partial N_{xx(t)}}{\partial x}=M\frac{\partial^2 u}{\partial t^2}+\kappa_{nf1}^2 MU^2\frac{\partial^2 u}{\partial x^2}+2\kappa_{nf1}MU\frac{\partial^2 u}{\partial t\partial x}+m\frac{\partial^2 u}{\partial t^2}, \tag{18}$$

$$\begin{aligned}&\frac{\partial}{\partial x}\left(N_{xx(t)}\frac{\partial w}{\partial x}\right)+\frac{\partial^2 M_{xx(t)}}{\partial x^2}=-F(x)\cos(\omega t)\\&M\frac{\partial^2 w}{\partial t^2}+\kappa_{nf1}^2 MU^2\frac{\partial^2 w}{\partial x^2}+2\kappa_{nf1}MU\frac{\partial^2 w}{\partial t\partial x}+m\frac{\partial^2 w}{\partial t^2}.\end{aligned} \tag{19}$$

Assuming a constant loading amplitude ($F(x)=F_1$) and substituting Eqs. (6) and (7) into Eqs. (18) and (19), one obtains the nonlinear coupled motion equations in the non-dimensional form as

$$\begin{aligned}&\frac{s}{r_A}\left[\frac{\partial^2 u}{\partial t^2}+2\kappa_{nf1}\sqrt{\bar{M}}U\frac{\partial^2 u}{\partial t\partial x}+\kappa_{nf1}^2U^2\frac{\partial^2 u}{\partial x^2}\right]\\&-\frac{s}{r_A}\chi_n^2\frac{\partial^2}{\partial x^2}\left[\frac{\partial^2 u}{\partial t^2}+2\kappa_{nf1}\sqrt{\bar{M}}U\frac{\partial^2 u}{\partial t\partial x}+\kappa_{nf1}^2U^2\frac{\partial^2 u}{\partial x^2}\right]\\&-\frac{\partial}{\partial x}\left[\frac{1}{2}\left(\frac{\partial w}{\partial x}\right)^2+s\frac{\partial u}{\partial x}\right]+\chi_g^2\frac{\partial^3}{\partial x^3}\left[s\frac{\partial u}{\partial x}+\frac{1}{2}\left(\frac{\partial w}{\partial x}\right)^2\right]\\&-\eta\frac{\partial}{\partial x}\left(s\frac{\partial^2 u}{\partial t\partial x}+\frac{\partial w}{\partial x}\frac{\partial^2 w}{\partial t\partial x}\right)+\eta\chi_g^2\frac{\partial^3}{\partial x^3}\left(s\frac{\partial^2 u}{\partial t\partial x}+\frac{\partial w}{\partial x}\frac{\partial^2 w}{\partial t\partial x}\right)=0,\end{aligned} \tag{20}$$

$$\begin{aligned}&\frac{\partial^2 w}{\partial t^2}+2\kappa_{nf1}\sqrt{\bar{M}}U\frac{\partial^2 w}{\partial t\partial x}+\kappa_{nf1}^2U^2\frac{\partial^2 w}{\partial x^2}\\&-\chi_n^2\frac{\partial^2}{\partial x^2}\left[\frac{\partial^2 w}{\partial t^2}+2\kappa_{nf1}\sqrt{\bar{M}}U\frac{\partial^2 w}{\partial t\partial x}+\kappa_{nf1}^2U^2\frac{\partial^2 w}{\partial x^2}\right]\\&+\frac{\partial^4 w}{\partial x^4}-\chi_g^2\frac{\partial^6 w}{\partial x^6}+\eta\frac{\partial^5 w}{\partial t\partial x^4}-\eta\chi_g^2\frac{\partial^7 w}{\partial t\partial x^6}-F_1\cos(\omega t)\\&-\frac{r_A}{s^2}\frac{\partial}{\partial x}\left\{\frac{\partial w}{\partial x}\left[\frac{1}{2}\left(\frac{\partial w}{\partial x}\right)^2+s\frac{\partial u}{\partial x}\right]-\chi_g^2\frac{\partial w}{\partial x}\frac{\partial^2}{\partial x^2}\left[\frac{1}{2}\left(\frac{\partial w}{\partial x}\right)^2+s\frac{\partial u}{\partial x}\right]\right.\\&\left.+\eta\frac{\partial w}{\partial x}\left(s\frac{\partial^2 u}{\partial t\partial x}+\frac{\partial w}{\partial x}\frac{\partial^2 w}{\partial t\partial x}\right)-\chi_g^2\eta\frac{\partial w}{\partial x}\frac{\partial^2}{\partial x^2}\left(s\frac{\partial^2 u}{\partial t\partial x}+\frac{\partial w}{\partial x}\frac{\partial^2 w}{\partial t\partial x}\right)\right.\end{aligned}$$

$$
\begin{aligned}
&+\frac{s}{r_A}\chi_n^2\frac{\partial w}{\partial x}\left[\frac{\partial^3 u}{\partial x\partial t^2}+2\kappa_{nf1}\sqrt{\bar{M}}U\frac{\partial^3 u}{\partial t\partial x^2}+\kappa_{nf1}^2U^2\frac{\partial^3 u}{\partial x^3}\right]\Bigg\}\\
&+\frac{r_A}{s^2}\chi_n^2\frac{\partial^3}{\partial x^3}\Bigg\{\frac{\partial w}{\partial x}\left[\frac{1}{2}\left(\frac{\partial w}{\partial x}\right)^2+s\frac{\partial u}{\partial x}\right]-\chi_g^2\frac{\partial w}{\partial x}\frac{\partial^2}{\partial x^2}\left[\frac{1}{2}\left(\frac{\partial w}{\partial x}\right)^2+s\frac{\partial u}{\partial x}\right]\\
&+\eta\frac{\partial w}{\partial x}\left(s\frac{\partial^2 u}{\partial x\partial t}+\frac{\partial w}{\partial x}\frac{\partial^2 w}{\partial t\partial x}\right)-\eta\chi_g^2\frac{\partial w}{\partial x}\frac{\partial^2}{\partial x^2}\left(s\frac{\partial^2 u}{\partial t\partial x}+\frac{\partial w}{\partial x}\frac{\partial^2 w}{\partial t\partial x}\right)\\
&+\frac{s}{r_A}\chi_n^2\frac{\partial w}{\partial x}\left[\frac{\partial^3 u}{\partial x\partial t^2}+2\kappa_{nf1}\sqrt{\bar{M}}U\frac{\partial^3 u}{\partial t\partial x^2}+\kappa_{nf1}^2U^2\frac{\partial^3 u}{\partial x^3}\right]\Bigg\}=0,
\end{aligned}
\tag{21}
$$

where

$$
\begin{aligned}
&\left\langle u^*,w^*\right\rangle=\frac{1}{d_o}\left\langle u,w\right\rangle,\ F^*=\frac{FL^4}{EId_o},\ \bar{M}=\frac{M}{m+M},\\
&\left\langle \chi_n,\chi_g\right\rangle=\frac{1}{L}\left\langle e_0l_n,l_g\right\rangle,\ \bar{\nabla}^2=\frac{\partial^2}{\partial x^{*2}},\ x^*=\frac{x}{L},\\
&t^*=\frac{t}{L^2}\left(\frac{EI}{m+M}\right)^{\frac{1}{2}},\quad \left\langle r_A,s\right\rangle=\left\langle\frac{AL^2}{I},\frac{L}{d_o}\right\rangle,\\
&\eta^*=\frac{\eta}{EL^2}\left(\frac{EI}{m+M}\right)^{\frac{1}{2}},\ \omega^*=\omega L^2\left(\frac{m+M}{EI}\right)^{\frac{1}{2}},\ U^*=UL\left(\frac{M}{EI}\right)^{\frac{1}{2}}.
\end{aligned}
\tag{22}
$$

In Eqs. (20) and (21), asterisk superscripts are ignored for simplicity. Using a discretisation technique based on Galerkin's method, one has

$$
u=\sum_{k=1}^{N_x}\phi_k(x)r_k(t),
\tag{23}
$$

$$
w=\sum_{k=1}^{N_z}\psi_k(x)q_k(t),
\tag{24}
$$

in which ϕ_j, r_j, ψ_j and q_j, respectively, represent the axial trial function, axial generalised coordinate, transverse trial function and transverse generalised coordinate. The boundary conditions of the fluid-conveying nanotube are assumed to be clamped-clamped as shown in Fig. 1. Substituting Eqs. (23) and (24) into Eqs. (20) and (21) leads to the following set of equations for the viscoelastic NSGT nanoscale tube conveying fluid

$$\frac{s}{r_A}\left\{\sum_{j=1}^{N_x}\left(\int_0^1\phi_k\phi_j dx\right)\frac{d^2r_j}{dt^2}+2\kappa_{nf1}\sqrt{\bar{M}}U\sum_{j=1}^{N_x}\left(\int_0^1\phi_k\frac{d\phi_j}{dx}dx\right)\frac{dr_j}{dt}\right.$$
$$\left.+\kappa_{nf1}^2U^2\sum_{j=1}^{N_x}\left(\int_0^1\phi_k\frac{d^2\phi_j}{dx^2}dx\right)r_j\right\}-\frac{s\chi_n^2}{r_A}\left\{\sum_{j=1}^{N_x}\left(\phi_k\int_0^1\frac{d^2\phi_j}{dx^2}dx\right)\frac{d^2r_j}{dt^2}\right.$$
$$\left.+2\kappa_{nf1}\sqrt{\bar{M}}U\sum_{j=1}^{N_x}\left(\int_0^1\phi_k\frac{d^3\phi_j}{dx^3}dx\right)\frac{dr_j}{dt}+\kappa_{nf1}^2U^2\sum_{j=1}^{N_x}\left(\int_0^1\phi_k\frac{d^4\phi_j}{dx^4}dx\right)r_j\right\}$$
$$-\int_0^1\phi_k\frac{d}{dx}\left(s\sum_{j=1}^{N_x}\frac{d\phi_j}{dx}r_j+\frac{1}{2}\sum_{j=1}^{N_z}\sum_{i=1}^{N_z}\frac{d\psi_j}{dx}\frac{d\psi_i}{dx}q_iq_j\right)dx$$
$$+\chi_g^2\int_0^1\phi_k\frac{d^3}{dx^3}\left(s\sum_{j=1}^{N_x}\frac{d\phi_j}{dx}r_j+\frac{1}{2}\sum_{j=1}^{N_z}\sum_{i=1}^{N_z}\frac{d\psi_i}{dx}\frac{d\psi_j}{dx}q_iq_j\right)dx$$
$$-\eta\int_0^1\phi_k\frac{d}{dx}\left(s\sum_{j=1}^{N_x}\frac{d\phi_j}{dx}\frac{dr_j}{dt}+\sum_{i=1}^{N_z}\sum_{j=1}^{N_z}\frac{d\psi_i}{dx}\frac{d\psi_j}{dx}q_i\frac{dq_j}{dt}\right)dx$$
$$+\eta\chi_g^2\int_0^1\phi_k\frac{d^3}{dx^3}\left(s\sum_{j=1}^{N_x}\frac{d\phi_j}{dx}\frac{dr_j}{dt}+\sum_{i=1}^{N_z}\sum_{j=1}^{N_z}\frac{d\psi_i}{dx}\frac{d\psi_j}{dx}q_i\frac{dq_j}{dt}\right)dx=0, \qquad (25)$$

$$
\begin{aligned}
&\sum_{j=1}^{N_z}\left(\int_0^1 \psi_k\psi_j dx\right)\frac{d^2q_j}{dt^2}+2\kappa_{nf1}\sqrt{\bar{M}}U\sum_{j=1}^{N_z}\left(\int_0^1 \psi_k\frac{d\psi_j}{dx}dx\right)\frac{dq_j}{dt}\\
&+\kappa_{nf1}^2U^2\sum_{j=1}^{N_z}\left(\int_0^1 \psi_k\frac{d^2\psi_j}{dx^2}dx\right)q_j-\chi_n^2\left\{\sum_{j=1}^{N_z}\left(\int_0^1 \psi_k\frac{d^2\psi_j}{dx^2}dx\right)\frac{d^2q_j}{dt^2}\right.\\
&\left.+2\kappa_{nf1}\sqrt{\bar{M}}U\sum_{j=1}^{N_z}\left(\int_0^1 \psi_k\frac{d^3\psi_j}{dx^3}dx\right)\frac{dq_j}{dt}+\kappa_{nf1}^2U^2\sum_{j=1}^{N_z}\left(\int_0^1 \psi_k\frac{d^4\psi_j}{dx^4}dx\right)q_j\right\}\\
&+\sum_{j=1}^{N_z}\left(\int_0^1 \psi_k\frac{d^4\psi_j}{dx^4}dx\right)q_j-\chi_g^2\sum_{j=1}^{N_z}\left(\int_0^1 \psi_k\frac{d^6\psi_j}{dx^6}dx\right)q_j-F_1\cos(\omega t)\left(\int_0^1 \psi_k dx\right)\\
&+\eta\sum_{j=1}^{N_z}\left(\int_0^1 \psi_k\frac{d^4\psi_j}{dx^4}dx\right)\frac{dq_j}{dt}-\eta\chi_g^2\sum_{j=1}^{N_z}\left(\int_0^1 \psi_k\frac{d^6\psi_j}{dx^6}dx\right)\frac{dq_j}{dt}\\
&-\frac{r_A}{s^2}\int_0^1\left\{\psi_k\frac{d}{dx}\left[\left(\sum_{j=1}^{N_z}\frac{d\psi_j}{dx}q_j\right)\left(s\sum_{j=1}^{N_x}\frac{d\phi_j}{dx}r_j+\frac{1}{2}\sum_{i=1}^{N_z}\sum_{j=1}^{N_z}\frac{d\psi_j}{dx}\frac{d\psi_i}{dx}q_iq_j\right)\right.\right.\\
&-\chi_g^2\left(\sum_{j=1}^{N_z}\frac{d\psi_j}{dx}q_j\right)\frac{d^2}{dx^2}\left(s\sum_{j=1}^{N_x}\frac{d\phi_j}{dx}r_j+\frac{1}{2}\sum_{i=1}^{N_z}\sum_{j=1}^{N_z}\frac{d\psi_j}{dx}\frac{d\psi_i}{dx}q_iq_j\right)\\
&+\eta\left(\sum_{j=1}^{N_z}\frac{d\psi_j}{dx}q_j\right)\left(s\sum_{j=1}^{N_x}\frac{d\phi_j}{dx}\frac{dr_j}{dt}+\sum_{i=1}^{N_z}\sum_{j=1}^{N_z}\frac{d\psi_j}{dx}\frac{d\psi_i}{dx}q_i\frac{dq_j}{dt}\right)\\
&-\chi_g^2\eta\left(\sum_{j=1}^{N_z}\frac{d\psi_j}{dx}q_j\right)\frac{d^2}{dx^2}\left(s\sum_{j=1}^{N_x}\frac{d\phi_j}{dx}\frac{dr_j}{dt}+\sum_{i=1}^{N_z}\sum_{j=1}^{N_z}\frac{d\psi_j}{dx}\frac{d\psi_i}{dx}q_i\frac{dq_j}{dt}\right)\\
&\left.\left.+\frac{s\chi_n^2}{r_A}\left(\sum_{j=1}^{N_z}\frac{d\psi_j}{dx}q_j\right)\left(\sum_{j=1}^{N_x}\frac{d\phi_j}{dx}\frac{d^2r_j}{dt^2}+2\kappa_{nf1}\sqrt{\bar{M}}U\sum_{j=1}^{N_x}\frac{d^2\phi_j}{dx^2}\frac{dr_j}{dt}+\kappa_{nf1}^2U^2\sum_{j=1}^{N_x}\frac{d^3\phi_j}{dx^3}r_j\right)\right]\right\}dx\\
&+\frac{r_A\chi_n^2}{s^2}\int_0^1\left\{\psi_k\frac{d^3}{dx^3}\left[\left(\sum_{j=1}^{N_z}\frac{d\psi_j}{dx}q_j\right)\left(s\sum_{j=1}^{N_x}\frac{d\phi_j}{dx}r_j+\frac{1}{2}\sum_{i=1}^{N_z}\sum_{j=1}^{N_z}\frac{d\psi_j}{dx}\frac{d\psi_i}{dx}q_iq_j\right)\right.\right.\\
&-\chi_g^2\left(\sum_{j=1}^{N_z}\frac{d\psi_j}{dx}q_j\right)\frac{d^2}{dx^2}\left(s\sum_{j=1}^{N_x}\frac{d\phi_j}{dx}r_j+\frac{1}{2}\sum_{i=1}^{N_z}\sum_{j=1}^{N_z}\frac{d\psi_j}{dx}\frac{d\psi_i}{dx}q_iq_j\right)\\
&+\eta\left(\sum_{j=1}^{N_z}\frac{d\psi_j}{dx}q_j\right)\left(s\sum_{j=1}^{N_x}\frac{d\phi_j}{dx}\frac{dr_j}{dt}+\sum_{i=1}^{N_z}\sum_{j=1}^{N_z}\frac{d\psi_j}{dx}\frac{d\psi_i}{dx}q_i\frac{dq_j}{dt}\right)\\
&-\eta\chi_g^2\left(\sum_{j=1}^{N_z}\frac{d\psi_j}{dx}q_j\right)\frac{d^2}{dx^2}\left(s\sum_{j=1}^{N_x}\frac{d\phi_j}{dx}\frac{dr_j}{dt}+\sum_{i=1}^{N_z}\sum_{j=1}^{N_z}\frac{d\psi_j}{dx}\frac{d\psi_i}{dx}q_i\frac{dq_j}{dt}\right)\\
&\left.\left.+\frac{s\chi_n^2}{r_A}\left(\sum_{j=1}^{N_z}q_j\frac{d\psi_j}{dx}\right)\left(\sum_{j=1}^{N_x}\frac{d\phi_j}{dx}\frac{d^2r_j}{dt^2}+2\kappa_{nf1}\sqrt{\bar{M}}U\sum_{j=1}^{N_x}\frac{d^2\phi_j}{dx^2}\frac{dr_j}{dt}+\kappa_{nf1}^2U^2\sum_{j=1}^{N_x}\frac{d^3\phi_j}{dx^3}r_j\right)\right]\right\}dx=0.
\end{aligned}
\tag{26}
$$

To predict the dynamic behaviour of viscoelastic NSGT nanotubes conveying nanofluid, a continuation technique is utilised.

3. Results and discussion

For numerical calculations, the geometric properties of the fluid-conveying nanoscale tube are taken as R_o =200.5 nm, h=70.0 nm and L/d_o=20. Furthermore, for the material properties, we have E=610 MPa, v=0.3 and density=1024 kg/m^3. Unless otherwise specified, the dimensionless parameters are as Kn=0.02, $\bar{M}$=0.4179, $\chi_g = 0.04$, $\chi_n = 0.10$, η=0.0004 and s=20.0. The number of trial functions along each axis is set to ten.

Figure 2 depicts the static divergence of the tube conveying nanofluid; midpoint transverse displacement versus the nanofluid velocity is plotted. The transverse displacement of the nanotube is zero until a critical point in which it starts to bifurcate. The critical velocity related to instability with slip boundary conditions using the NSGT is obtained as U_{cr} = 4.6932.

The effect of the nonlocal and strain gradient parameters on the static divergence of the tube conveying nanofluid is depicted in Fig. 3. To better illustrate the size effects, in sub-figure (a) χ_n is kept fixed and the effect of χ_g is studied while in sub-figure (b) χ_g is kept fixed and the effect of χ_n is examined. As seen in sub-figure (a), increasing χ_g postpones the occurrence of divergence and increases the critical flow velocity. Increasing χ_n, on the other hand, results in a reduction in the critical flow velocity corresponding to divergence, as illustrated in sub-figure (b).

Figure 4 shows the nanosystem fundamental natural frequency in sub and supercritical flow regimes. It is found that in the subcritical flow regime, the fundamental frequency decreases with increasing the nanofluid velocity whereas it increases with increasing the velocity in the supercritical flow regime. Moreover, the fundamental frequency vanishes at the critical point corresponding to the nanosystem divergence.

The subcritical amplitude-frequency diagrams of the fluid-conveying tube at nanoscales are shown in Fig. 5 for the maximum displacement in the transverse axis at x=0.5, the maximum displacement in the longitudinal axis at x=0.657 and the minimum longitudinal displacement at x=0.344. The fluid-conveying nanoscale tube displays a hardening nonlinearity with strong modal interactions for both transverse and axial responses. There are two entirely different saddle-node points at ω/ω_1 = 1.2819 and 1.0591, in which the fluid-conveying nanoscale system undergoes a sudden jump in both transverse and axial displacements. Furthermore, the transverse and longitudinal responses of the fluid-conveying nanoscale tube of Fig. 5 in one period of oscillation at ω/ω_1 = 1.2819 are indicated in Fig. 6.

Figure 7 compares the subcritical frequency-amplitude diagrams of the fluid-conveying nanoscale tube obtained via the NSGT (χ_g=0.04, χ_n=0.10) with those of the classical theory (χ_g= χ_n=0) for the maximum displacement in the transverse axis at x=0.5 and the maximum displacement in the longitudinal axis at x=0.657. It is concluded that the application of the classical model results in overestimated values for the resonance frequency as well as the peak amplitude of the fluid-conveying nanotube. In addition, the classical model is not able to predict the modal interactions observed in the nonlinear frequency response for the longitudinal motion.

The subcritical frequency-amplitude diagrams of the fluid-conveying nanoscale tube for different fluid velocities are indicated in Fig. 8 for the maximum transverse displacement at x=0.5 as well as the maximum longitudinal displacement at x=0.657. It is observed that higher fluid velocities lead to lower resonance frequencies for the nanosystem. Furthermore, for a sufficiently high fluid velocity (i.e. U/U_{cr}=0.8) in the subcritical flow

regime, modal interactions are observed in the frequency response, especially for the longitudinal motion.

The slip effects at the nanotube-fluid interface on the subcritical amplitude-frequency diagrams of the fluid-conveying tube at nanoscales are shown in Fig. 9 for the maximum displacement in the transverse axis at x=0.5 as well as the maximum displacement in the longitudinal axis at x=0.657. Neglecting slip effects at the nanotube-fluid interface leads to notably higher resonance frequencies and peak amplitudes for the nanosystem. Furthermore, modal interactions are not observed in the nonlinear response when slip boundary conditions are neglected.

Figure 10 illustrates the supercritical frequency-amplitude diagrams of nanoscale tubes conveying fluid of velocity U/U_{cr}=1.20 for the maximum and minimum transverse displacements at x=0.5 as well as the maximum displacement in longitudinal axis at x=0.657. The fluid-conveying nanoscale tube displays a softening nonlinearity for both transverse and axial responses. Furthermore, there are two saddle-node bifurcations at ω/ω_1=0.9514 and 0.7963 in the nonlinear frequency response in which the nanosystem displays a sudden jump in the amplitude. The effects of a slight increase in the fluid velocity on the frequency response are shown in Fig. 11; this time the fluid velocity is set to U/U_{cr}=1.40. It is found that a slight increase in the nanofluid velocity leads to the dramatic change of the frequency response of viscoelastic nanoscale tubes. There are four saddle-node bifurcations (i.e. SD_1: ω/ω_1=0.9446, SD_2: ω/ω_1=0.9290, SD_3: ω/ω_1=1.7984, SD_4: ω/ω_1=2.0598,) and two period-doubling bifurcations (i.e. PD_1: ω/ω_1=1.9234, PD_2: ω/ω_1=2.0587). Finally, the effects of the velocity correction factor on the supercritical amplitude-frequency diagrams of the nanofluid-conveying nanoscale tube are shown in Fig. 12 for the maximum displacement in

the transverse axis at x=0.5 and the maximum displacement in the longitudinal axis at x=0.657. The resonance frequency is higher for higher velocity correction factors.

4. Conclusions

A nonlinear viscoelastic model has been developed for the frequency response of nanotubes conveying fluid incorporating both transverse deflections and axial displacements. Both strain gradients and stress nonlocality were taken into consideration via a NSGT model. The occurrence of slip in the interface between the fluid and nanotube was modelled employing the Beskok-Karniadakis theory. The effects of viscoelastic properties on the nonlinear frequency response were captured using the Kelvin-Voigt model. Galerkin's technique and a continuation scheme were applied to determine a numerical solution.

It was found that in the subcritical flow regime, increasing the nanofluid velocity reduces the fundamental frequency while the velocity has an increasing impact on the fundamental frequency in the supercritical flow regime. For both transverse and axial responses, the fluid-conveying nanosystem displays a hardening nonlinearity with strong modal interactions in the subcritical regime. Furthermore, employing the classical model results in overestimated values for the resonance frequencies and peak amplitudes of the nanoscale tube. Higher fluid velocities lead to lower resonance frequencies. In addition, it was observed that neglecting slip boundary conditions leads to significantly higher resonance frequencies and peak amplitudes. In the supercritical flow regime, the fluid-conveying nanoscale tube displays a softening nonlinearity for both transverse and axial responses.

Conflict of interest statement

The authors declare no conflict of interest in preparing this article.

Funding acknowledgement

This research received no specific grant from any funding agency in the public, commercial, or not-for-profit sectors.

References

Akgöz B and Civalek Ö. (2012) Free vibration analysis for single-layered graphene sheets in an elastic matrix via modified couple stress theory. *Materials & Design* 42: 164-171.

Arda M and Aydogdu M. (2018) Dynamic stability of harmonically excited nanobeams including axial inertia. *Journal of Vibration and Control*: 1077546318802430.

Asemi SR and Farajpour A. (2014) Vibration characteristics of double-piezoelectric-nanoplate-systems. *IET Micro & Nano Letters* 9(4): 280-285.

Askari H and Esmailzadeh E. (2017) Forced vibration of fluid conveying carbon nanotubes considering thermal effect and nonlinear foundations. *Composites Part B: Engineering* 113: 31-43.

Atashafrooz M, Bahaadini R and Sheibani HR. (2018) Nonlocal, strain gradient and surface effects on vibration and instability of nanotubes conveying nanoflow. *Mechanics of Advanced Materials and Structures*: 1-13.

Aydogdu M. (2015) A nonlocal rod model for axial vibration of double-walled carbon nanotubes including axial van der Waals force effects. *Journal of Vibration and Control* 21(16): 3132-3154.

Bahaadini R and Hosseini M. (2016) Nonlocal divergence and flutter instability analysis of embedded fluid-conveying carbon nanotube under magnetic field. *Microfluidics and Nanofluidics* 20(7): 108.

Beskok A and Karniadakis GE. (1999) Report: a model for flows in channels, pipes, and ducts at micro and nano scales. *Microscale Thermophysical Engineering* 3(1): 43-77.

Farajpour A, Ghayesh MH and Farokhi H. (2018a) A review on the mechanics of nanostructures. *International Journal of Engineering Science* 133: 231-263.

Farajpour A, Ghayesh MH and Farokhi H. (2019) Large-amplitude coupled scale-dependent behaviour of geometrically imperfect NSGT nanotubes. *International Journal of Mechanical Sciences* 150: 510-525.

Farajpour M, Shahidi A and Farajpour A. (2018b) A nonlocal continuum model for the biaxial buckling analysis of composite nanoplates with shape memory alloy nanowires. *Materials Research Express* 5(3): 035026.

Farokhi H and Ghayesh MH. (2015) Nonlinear dynamical behaviour of geometrically imperfect microplates based on modified couple stress theory. *International Journal of Mechanical Sciences* 90: 133-144.

Farokhi H and Ghayesh MH. (2017) Viscoelastic resonant responses of shear deformable imperfect microbeams. *Journal of Vibration and Control*: 1077546317699345.

Farokhi H and Ghayesh MH. (2018) Supercritical nonlinear parametric dynamics of Timoshenko microbeams. *Communications in Nonlinear Science and Numerical Simulation* 59: 592-605.

Farokhi H, Ghayesh MH, Gholipour A, et al. (2018) Modal interactions and energy transfers in large-amplitude vibrations of functionally graded microcantilevers. *Journal of Vibration and Control* 24(17): 3882-3893.
Ghasemi A, Dardel M, Ghasemi MH, et al. (2013) Analytical analysis of buckling and post-buckling of fluid conveying multi-walled carbon nanotubes. *Applied Mathematical Modelling* 37(7): 4972-4992.
Ghayesh MH and Farajpour A. (2018a) Nonlinear coupled mechanics of nanotubes incorporating both nonlocal and strain gradient effects. *Mechanics of Advanced Materials and Structures* doi: 10.1080/15376494.2018.1473537: 1-10.
Ghayesh MH and Farajpour A. (2018b) Nonlinear mechanics of nanoscale tubes via nonlocal strain gradient theory. *International Journal of Engineering Science* 129: 84-95.
Ghayesh MH, Farokhi H and Amabili M. (2013) Nonlinear behaviour of electrically actuated MEMS resonators. *International Journal of Engineering Science* 71: 137-155.
Ghayesh MH and Moradian N. (2011) Nonlinear dynamic response of axially moving, stretched viscoelastic strings. *Archive of Applied Mechanics* 81(6): 781-799.
Gholipour A, Farokhi H and Ghayesh MH. (2015) In-plane and out-of-plane nonlinear size-dependent dynamics of microplates. *Nonlinear Dynamics* 79(3): 1771-1785.
Hosseini M, Bahaadini R and Jamali B. (2018) Nonlocal instability of cantilever piezoelectric carbon nanotubes by considering surface effects subjected to axial flow. *JVC/Journal of Vibration and Control* 24(9): 1809-1825.
Kazemirad S, Ghayesh MH and Amabili M. (2013) Thermo-mechanical nonlinear dynamics of a buckled axially moving beam. *Archive of Applied Mechanics* 83(1): 25-42.
Kural S and Özkaya E. (2017) Size-dependent vibrations of a micro beam conveying fluid and resting on an elastic foundation. *JVC/Journal of Vibration and Control* 23(7): 1106-1114.
Lee H-L and Chang W-J. (2008) Free transverse vibration of the fluid-conveying single-walled carbon nanotube using nonlocal elastic theory. *Journal of applied physics* 103(2): 024302.
Li L and Hu Y. (2015) Buckling analysis of size-dependent nonlinear beams based on a nonlocal strain gradient theory. *International Journal of Engineering Science* 97: 84-94.
Li L and Hu Y. (2016) Wave propagation in fluid-conveying viscoelastic carbon nanotubes based on nonlocal strain gradient theory. *Computational Materials Science* 112: 282-288.
Liang F and Su Y. (2013) Stability analysis of a single-walled carbon nanotube conveying pulsating and viscous fluid with nonlocal effect. *Applied Mathematical Modelling* 37(10-11): 6821-6828.
Lim C, Zhang G and Reddy J. (2015) A higher-order nonlocal elasticity and strain gradient theory and its applications in wave propagation. *Journal of the Mechanics and Physics of Solids* 78: 298-313.
Malekzadeh P and Shojaee M. (2015) A two-variable first-order shear deformation theory coupled with surface and nonlocal effects for free vibration of nanoplates. *Journal of Vibration and Control* 21(14): 2755-2772.
Maraghi ZK, Arani AG, Kolahchi R, et al. (2013) Nonlocal vibration and instability of embedded DWBNNT conveying viscose fluid. *Composites Part B: Engineering* 45(1): 423-432.
Mehralian F, Beni YT and Zeverdejani MK. (2017a) Calibration of nonlocal strain gradient shell model for buckling analysis of nanotubes using molecular dynamics simulations. *Physica B: Condensed Matter* 521: 102-111.
Mehralian F, Beni YT and Zeverdejani MK. (2017b) Nonlocal strain gradient theory calibration using molecular dynamics simulation based on small scale vibration of nanotubes. *Physica B: Condensed Matter* 514: 61-69.
Mohammadi K, Rajabpour A and Ghadiri M. (2018) Calibration of nonlocal strain gradient shell model for vibration analysis of a CNT conveying viscous fluid using molecular dynamics simulation. *Computational Materials Science* 148: 104-115.

Mohammadimehr M, Mohammadi Hooyeh H, Afshari H, et al. (2017) Free vibration analysis of double-bonded isotropic piezoelectric Timoshenko microbeam based on strain gradient and surface stress elasticity theories under initial stress using differential quadrature method. *Mechanics of Advanced Materials and Structures* 24(4): 287-303.

Nejad MZ, Hadi A and Farajpour A. (2017) Consistent couple-stress theory for free vibration analysis of Euler-Bernoulli nano-beams made of arbitrary bi-directional functionally graded materials. *Structural Engineering and Mechanics* 63(2): 161-169.

Numanoğlu HM, Akgöz B and Civalek Ö. (2018) On dynamic analysis of nanorods. *International Journal of Engineering Science* 130: 33-50.

Oveissi S, Toghraie D and Eftekhari SA. (2016) Longitudinal vibration and stability analysis of carbon nanotubes conveying viscous fluid. *Physica E: Low-Dimensional Systems and Nanostructures* 83: 275-283.

Park S and Gao X. (2006) Bernoulli–Euler beam model based on a modified couple stress theory. *Journal of Micromechanics and Microengineering* 16(11): 2355.

Reddy J. (2010) Nonlocal nonlinear formulations for bending of classical and shear deformation theories of beams and plates. *International Journal of Engineering Science* 48(11): 1507-1518.

Soltani P, Taherian M and Farshidianfar A. (2010) Vibration and instability of a viscous-fluid-conveying single-walled carbon nanotube embedded in a visco-elastic medium. *Journal of Physics D: Applied Physics* 43(42): 425401.

Wang L. (2010) Size-dependent vibration characteristics of fluid-conveying microtubes. *Journal of Fluids and Structures* 26(4): 675-684.

Zeighampour H and Beni YT. (2014) Size-dependent vibration of fluid-conveying double-walled carbon nanotubes using couple stress shell theory. *Physica E: Low-Dimensional Systems and Nanostructures* 61: 28-39.

Zenkour A. (2018) Nonlocal elasticity and shear deformation effects on thermal buckling of a CNT embedded in a viscoelastic medium. *The European Physical Journal Plus* 133(5): 196.

Zhen Y-X, Fang B and Tang Y. (2011) Thermal–mechanical vibration and instability analysis of fluid-conveying double walled carbon nanotubes embedded in visco-elastic medium. *Physica E: Low-Dimensional Systems and Nanostructures* 44(2): 379-385.

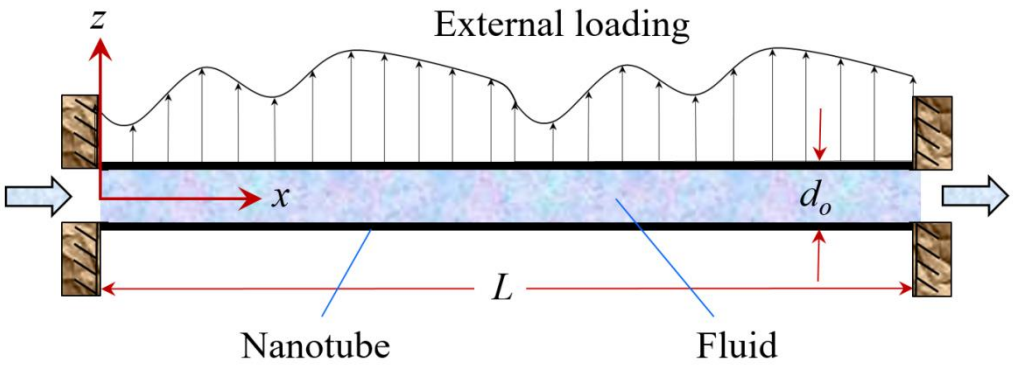

Fig. 1. A fluid-conveying nanoscale tube with outer diameter d_o and length L.

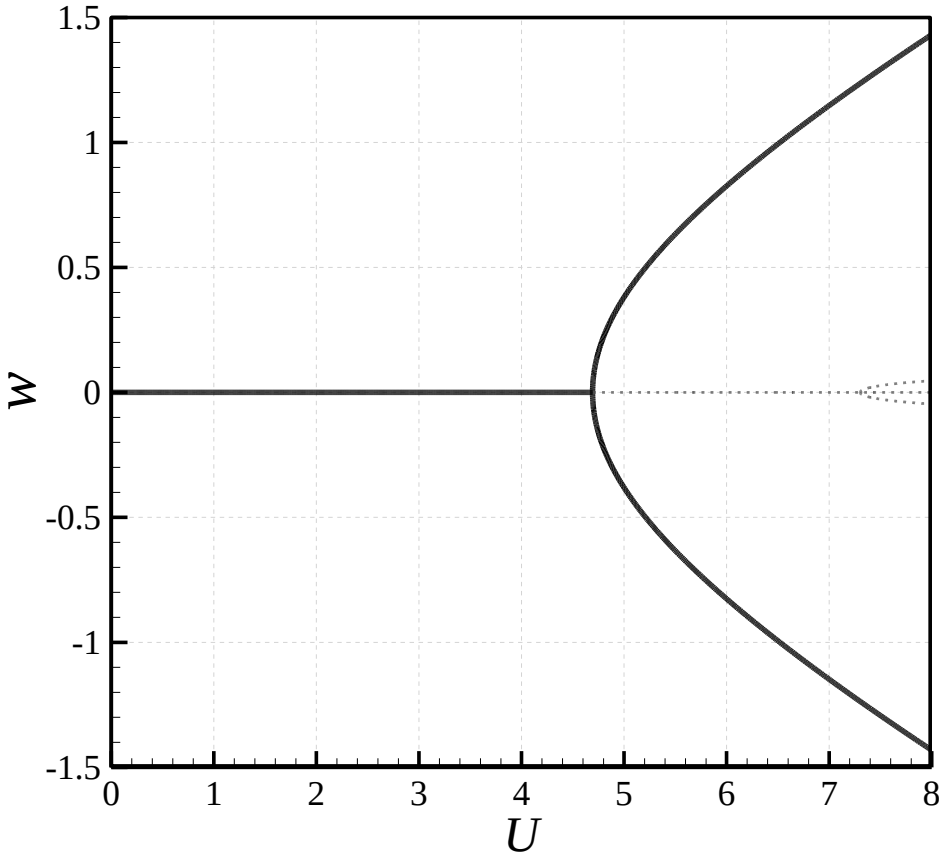

Fig. 2. Static divergence of the nanoscale tube conveying nanofluid; w at midpoint.

(a)

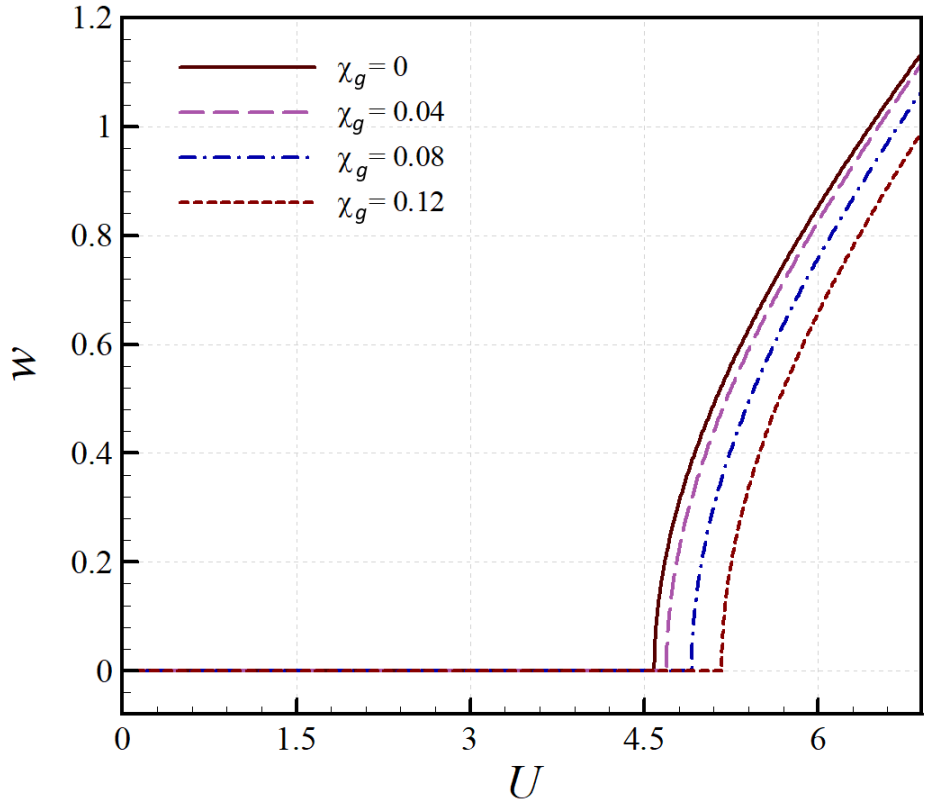

(b)

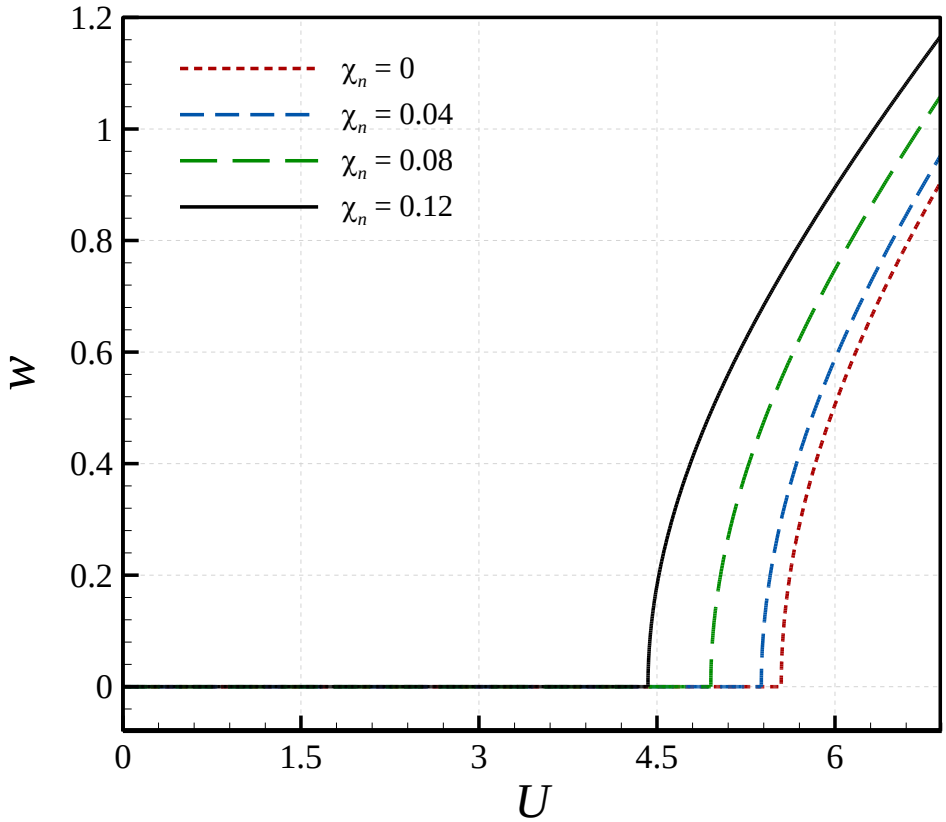

Fig. 3. Nonlocal and strain gradient effects on positive stable static response of the nanoscale tube conveying nanofluid at midpoint; (a) χ_n = 0.10; (b) χ_g = 0.04.

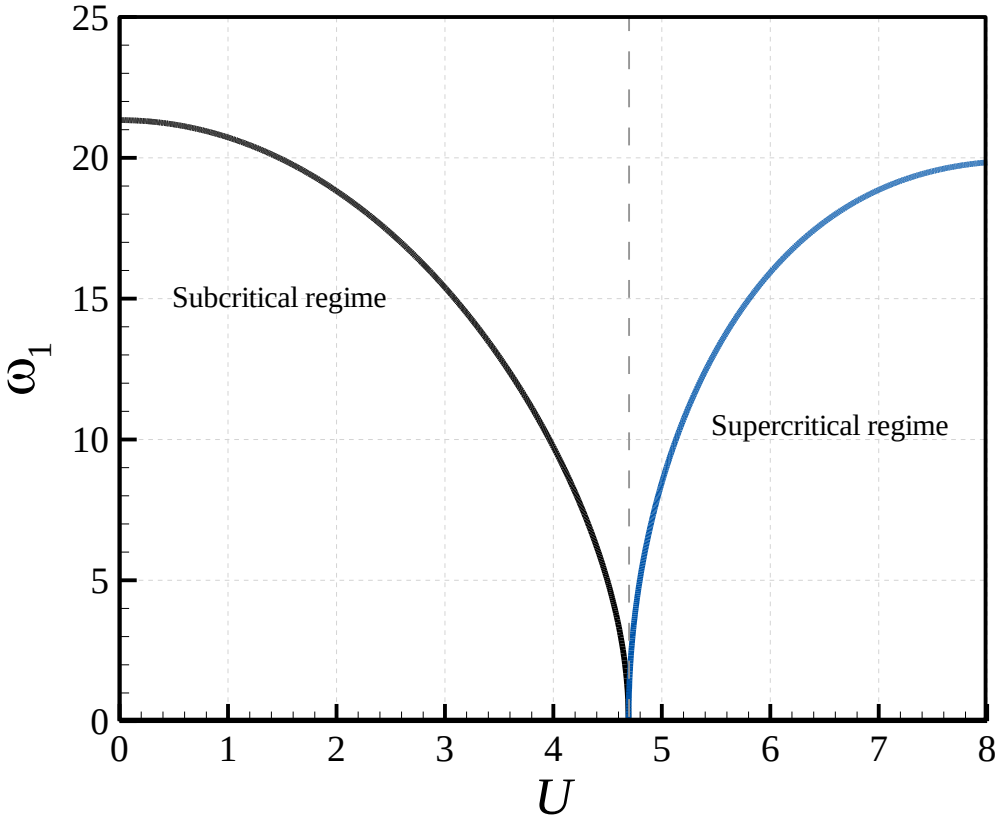

Fig. 4. Nanosystem fundamental natural frequency in sub and supercritical flow regimes; κ_{nf1}=1.1595.

(a)

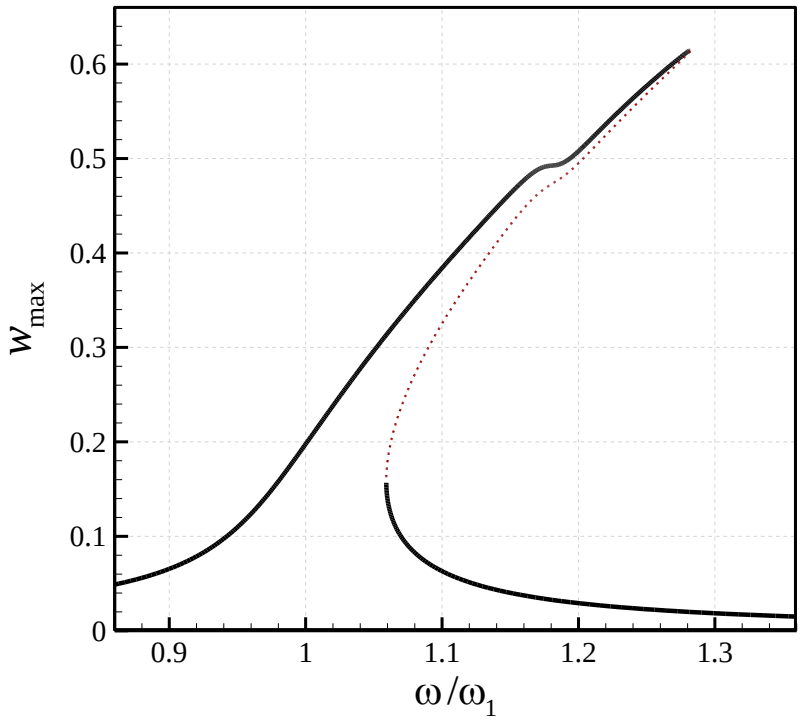
0.6
0.5
0.4
0.3
0.2
0.1
0
w_{max}
0.9
1
1.1
1.2
1.3
ω/ω_1

(b)

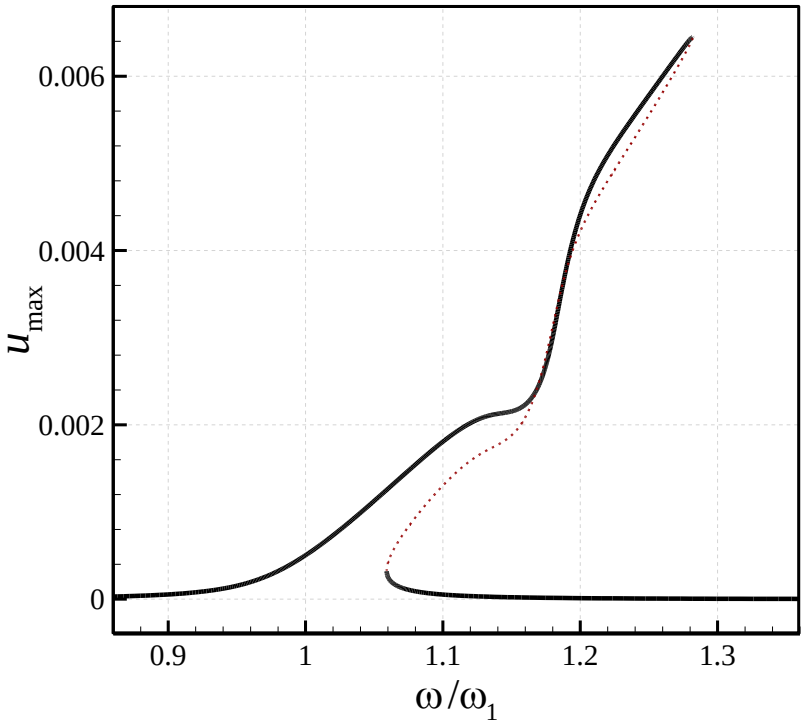
0.006
0.004
0.002
0
u_{max}
0.9
1
1.1
1.2
1.3
ω/ω_1

(c)

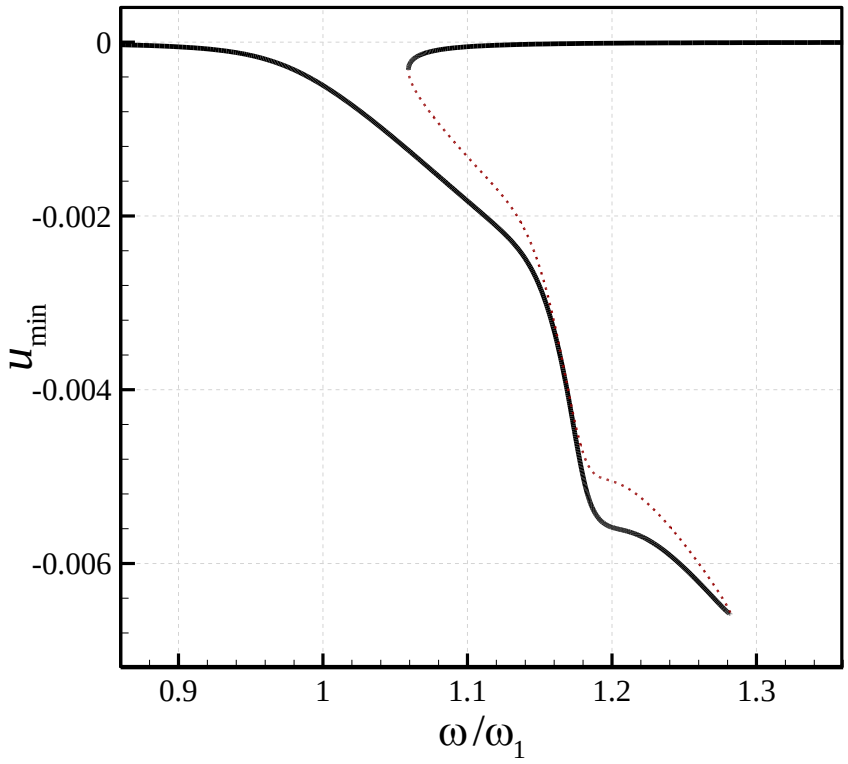

Fig. 5. Subcritical amplitude-frequency diagrams of the nanofluid-conveying nanoscale tube; (a) w_{max} at x=0.5; (b) u_{max} at x=0.657; (c) u_{min} at x=0.344; U/U_{cr}=0.75, κ_{nf1}=1.1595 and F_1=2.2.

(a)

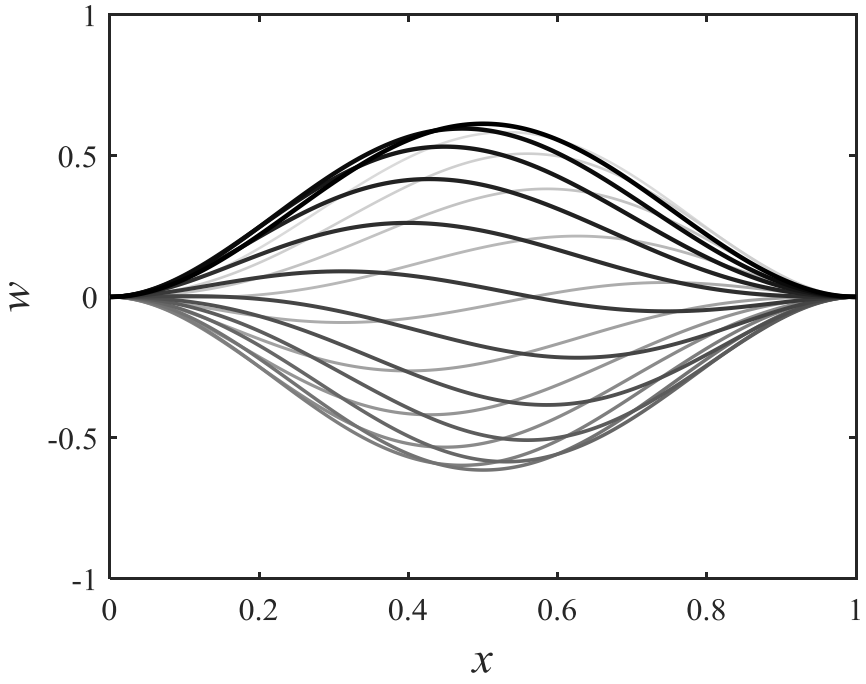

(b)

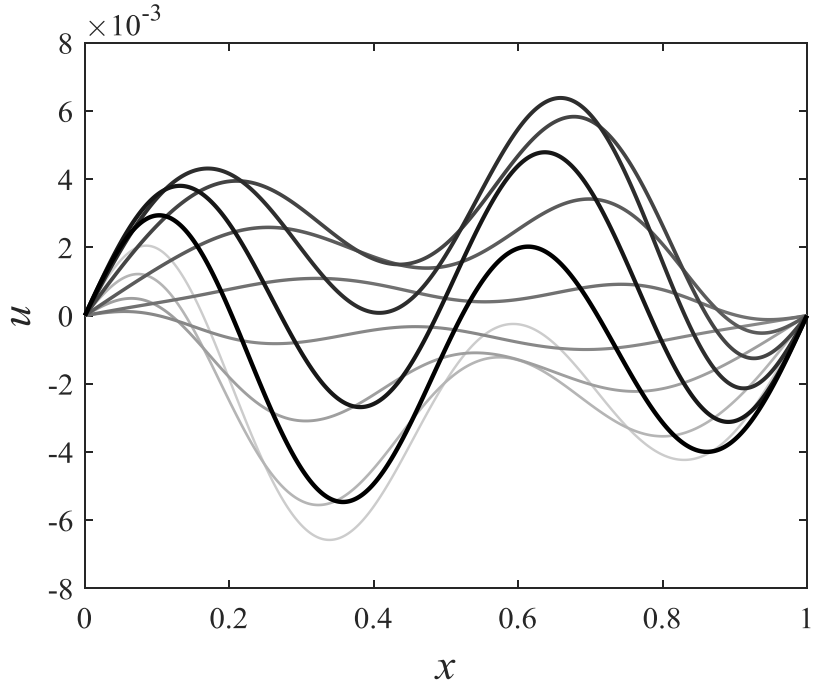

Fig. 6. (a, b) Transverse and longitudinal response of fluid-conveying nanotube of Fig. 4 in one period of oscillation at ω/ω_1 = 1.2819.

(a)

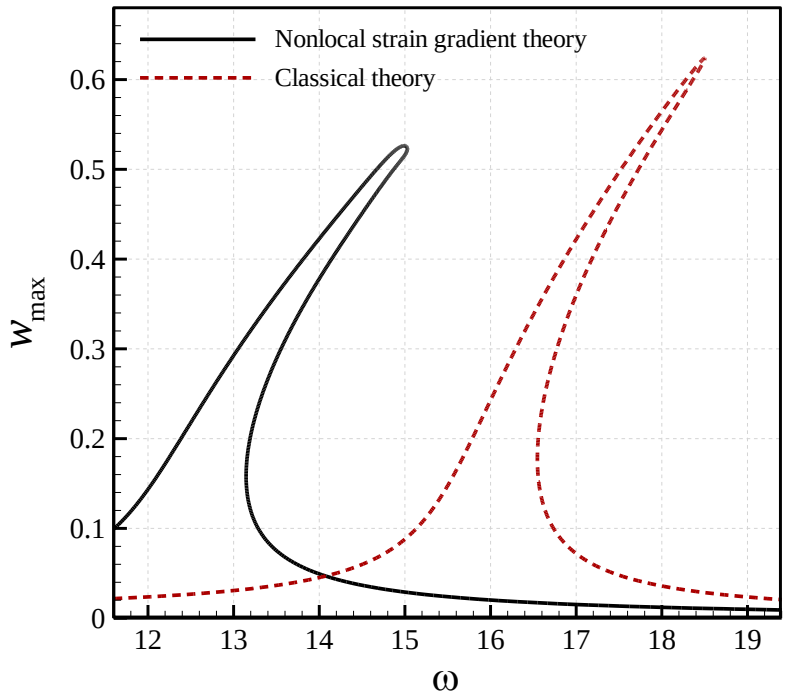

(b)

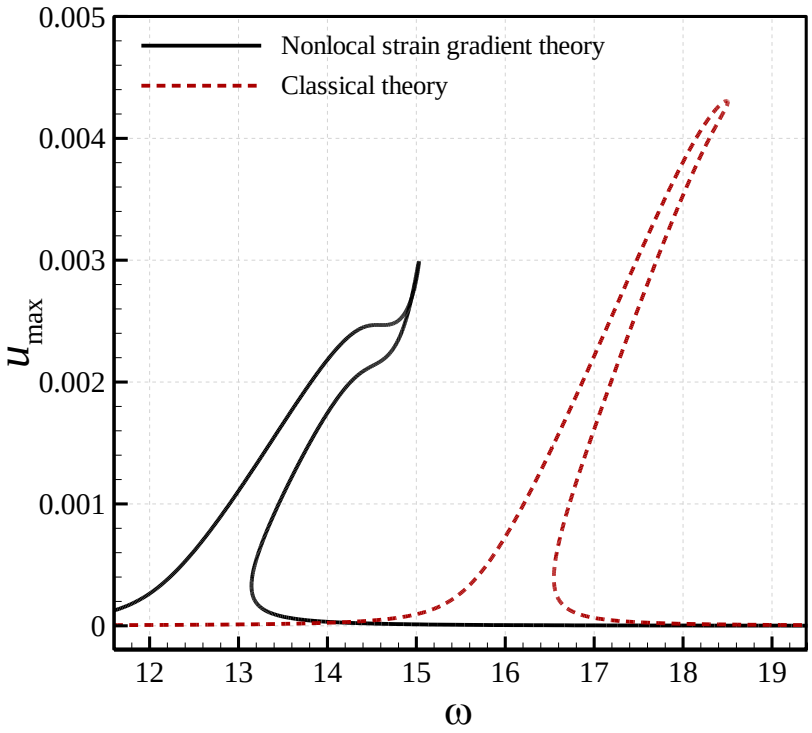

Fig. 7. Subcritical amplitude-frequency diagrams of the nanofluid-conveying nanoscale tube obtained via the nonlocal strain gradient theory (χ_g=0.04, χ_n=0.10) and classical theory (χ_g=χ_n=0); (a) w_{max} at x=0.5; (b) u_{max} at x=0.657; U=3.6, κ_{nf1}=1.1595 and F_1=2.2.

(a)

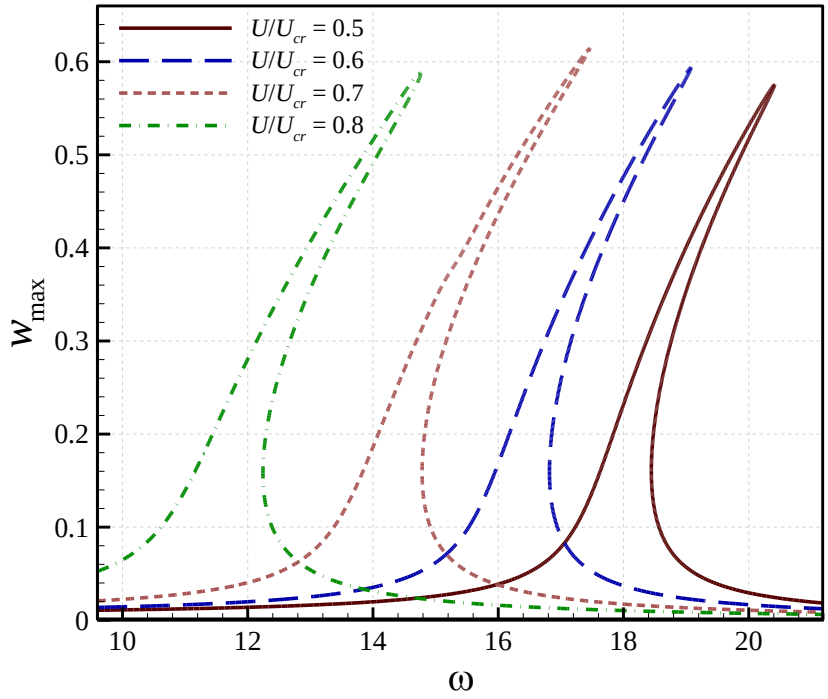

(b)

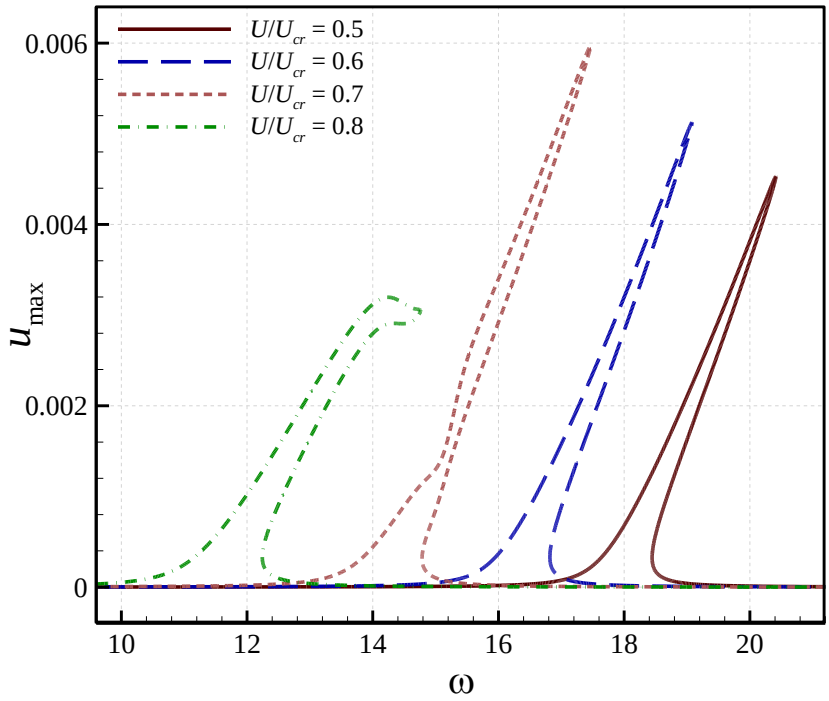

Fig. 8. Subcritical amplitude-frequency diagrams of the nanofluid-conveying nanoscale tube for different fluid speeds; (a) w_{max} at x=0.5; (b) u_{max} at x=0.657; κ_{nf1}=1.1595 and F_1=2.2.

(a)

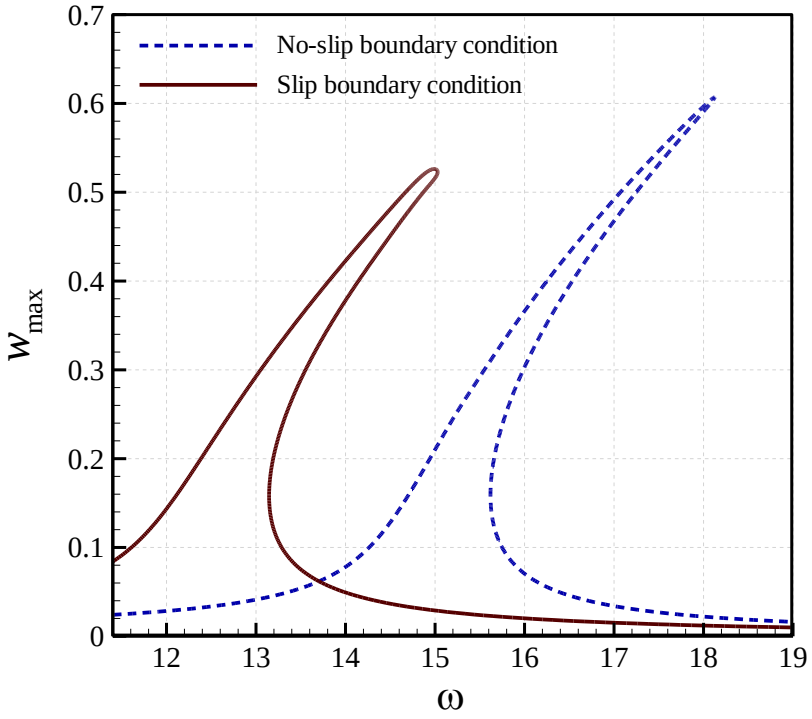

(b)

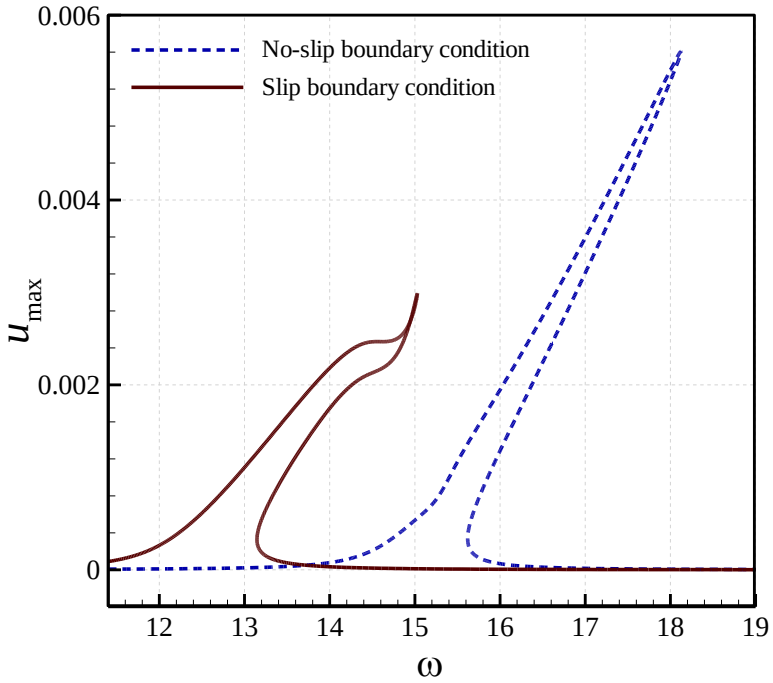

Fig. 9. Slip effects on subcritical amplitude-frequency diagrams of the nanofluid-conveying nanoscale tube; (a) w_{max} at x=0.5; (b) u_{max} at x=0.657; U=3.6 and F_1=2.2; κ_{nf1}=1.1595 for slip boundary condition and κ_{nf1}=1.0 for no-slip boundary condition.

(a)

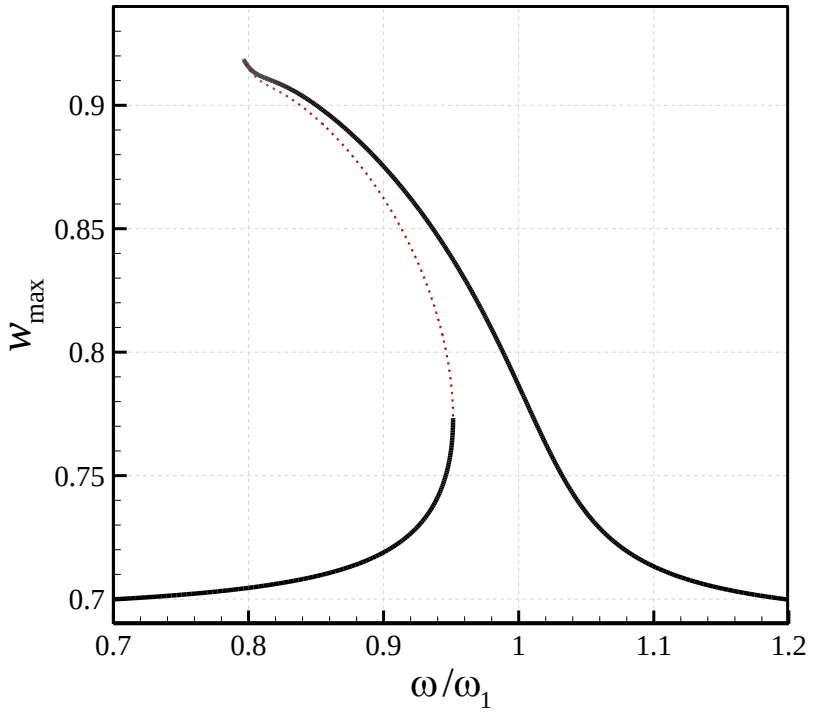
0.9
0.85
0.8
0.75
0.7
w_{max}
0.7
0.8
0.9
1
1.1
1.2
ω/ω_1

(b)

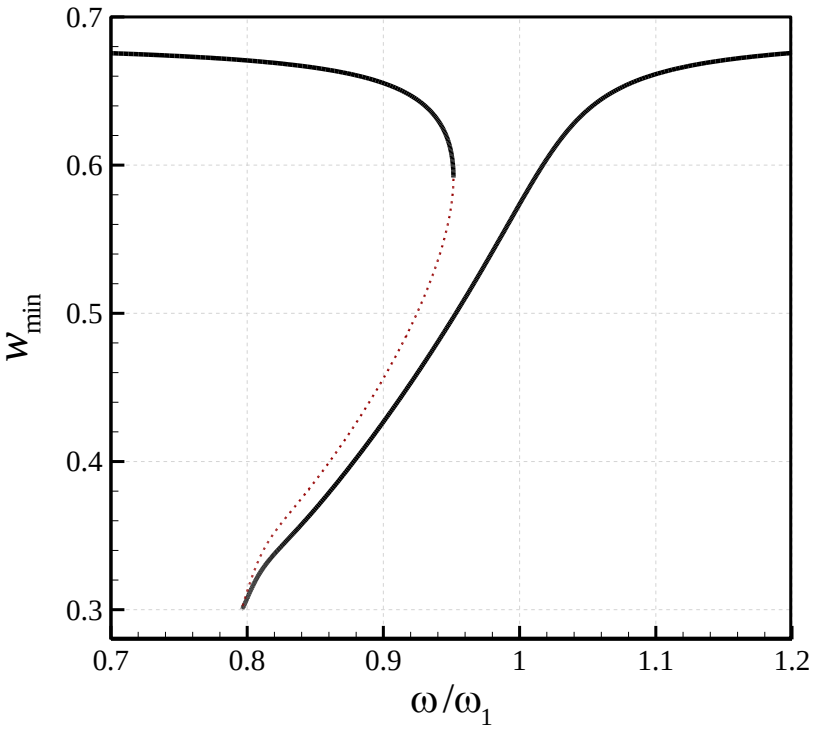
0.7
0.6
0.5
0.4
0.3
w_{min}
0.7
0.8
0.9
1
1.1
1.2
ω/ω_1

(c)

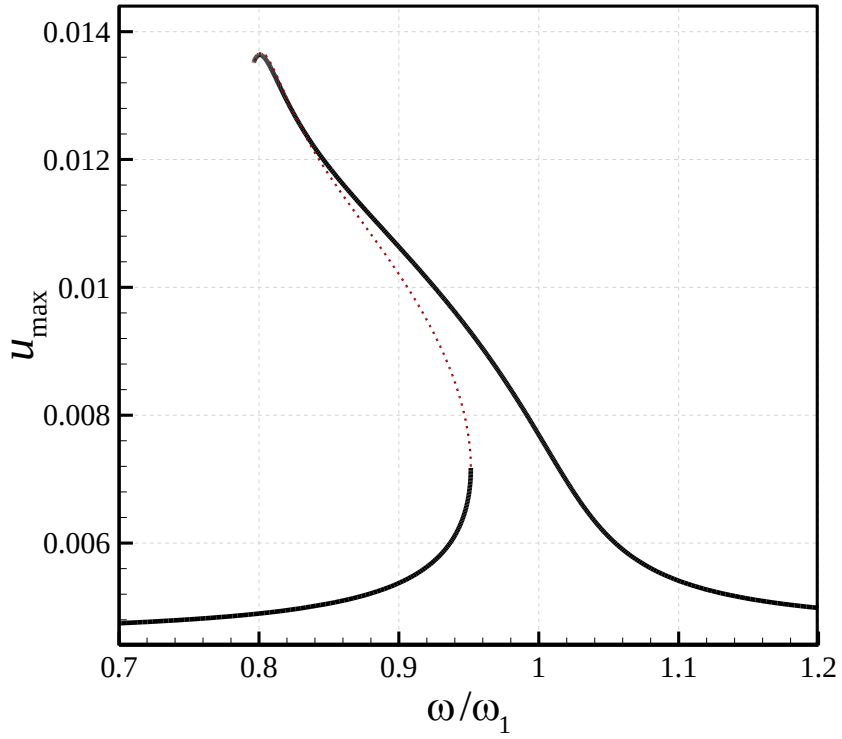

Fig. 10. Supercritical amplitude-frequency diagrams of the nanofluid-conveying nanoscale tube; (a,b) w_{max} and w_{min} at x=0.5; (c) u_{max} at x=0.657; U/U_{cr}=1.20, κ_{nf1}=1.1595 and F_1=2.2.

(a)

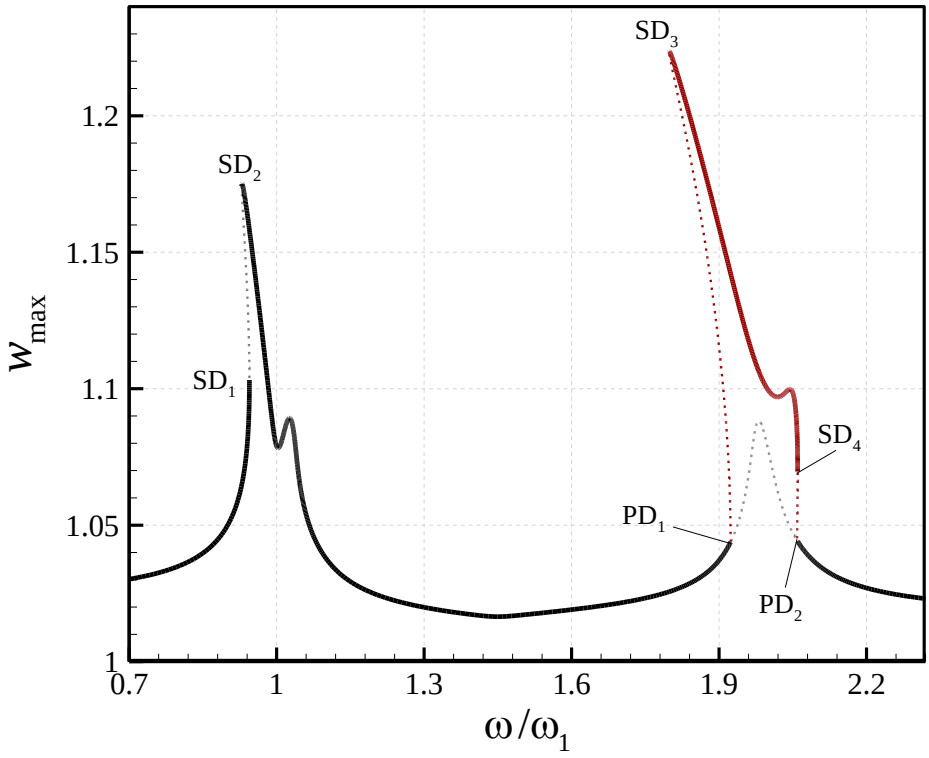
SD3
SD2
SD1
SD4
PD1
PD2
1.2
1.15
1.1
1.05
1
0.7
1
1.3
1.6
1.9
2.2
wmax
ω/ω1

(b)

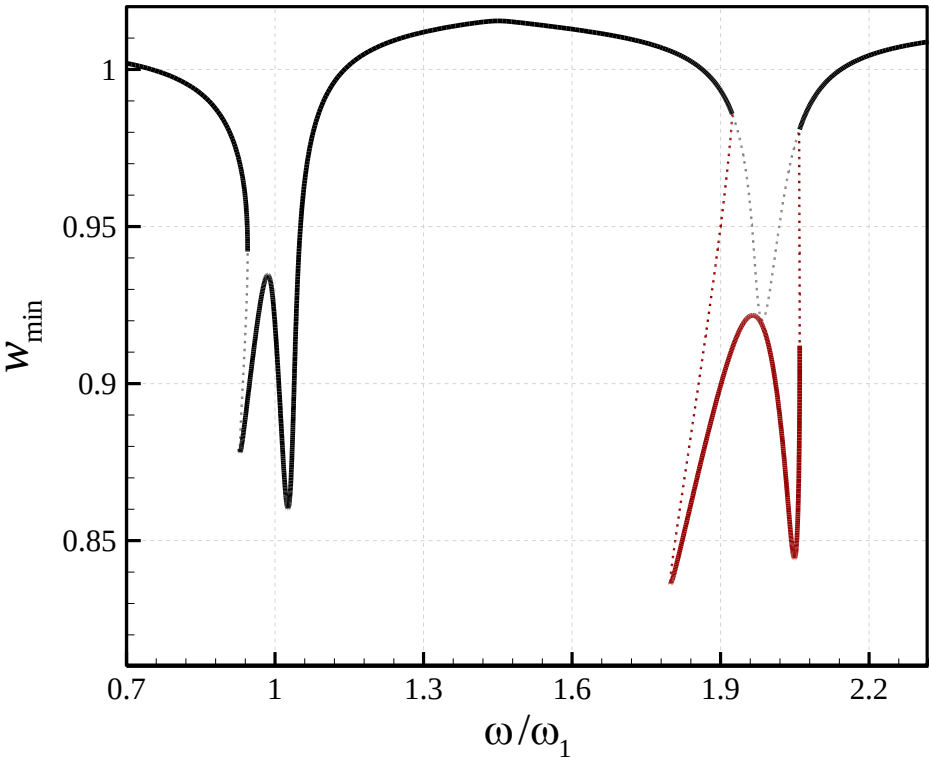
1
0.95
0.9
0.85
0.7
1
1.3
1.6
1.9
2.2
wmin
ω/ω1

(c)

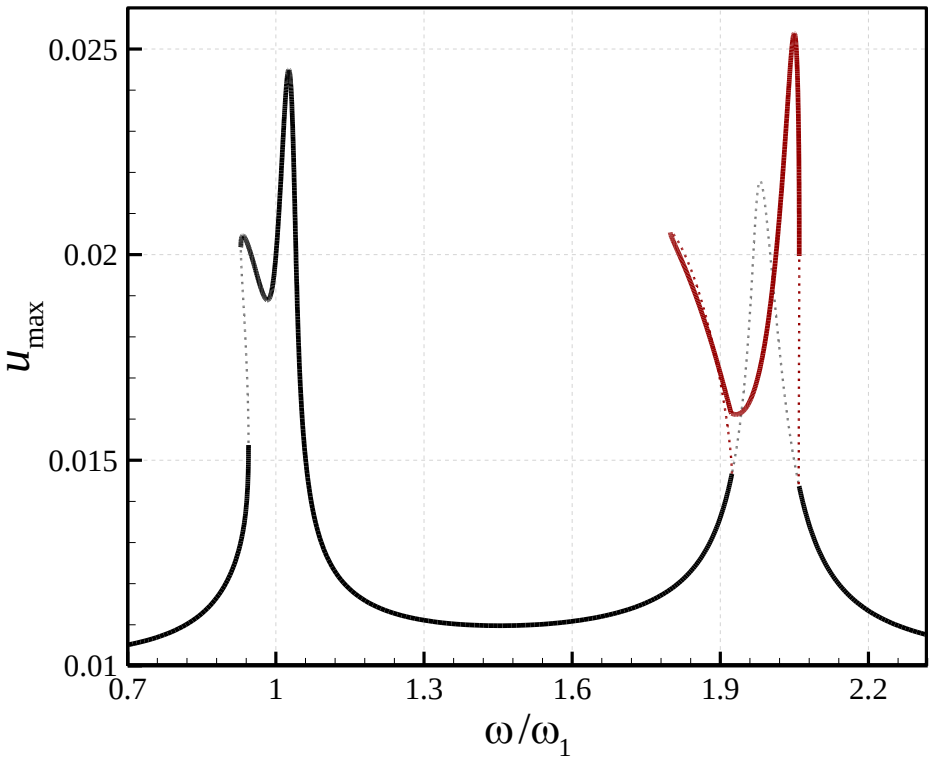

Fig. 11. Supercritical amplitude-frequency diagrams of the nanofluid-conveying nanoscale tube; (a) w_{max} and w_{min} at x=0.5; (b) u_{max} at x=0.657; U/U_{cr}=1.40, κ_{nf1}=1.1595, and F_1=6.0.

(a)

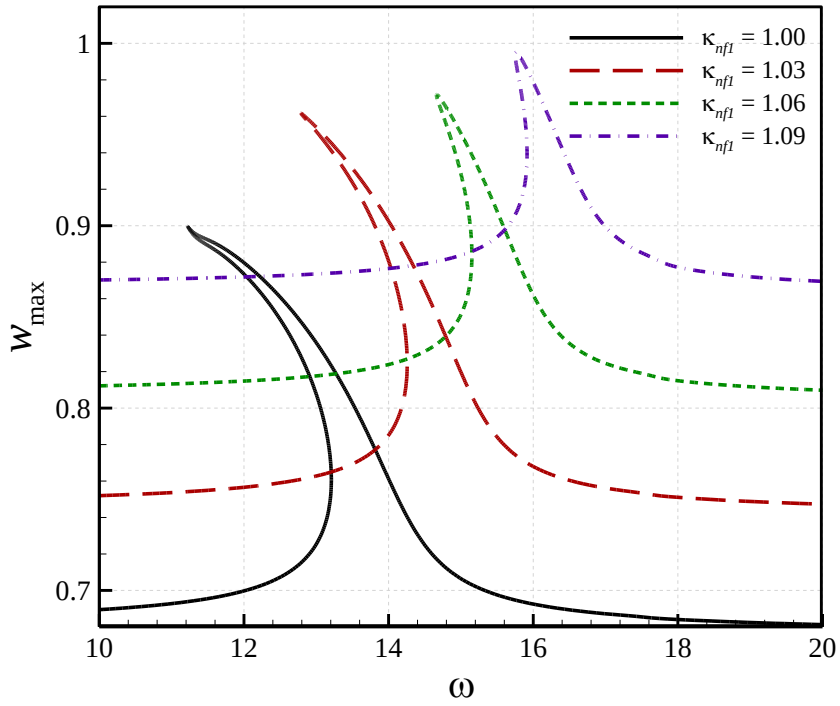

(b)

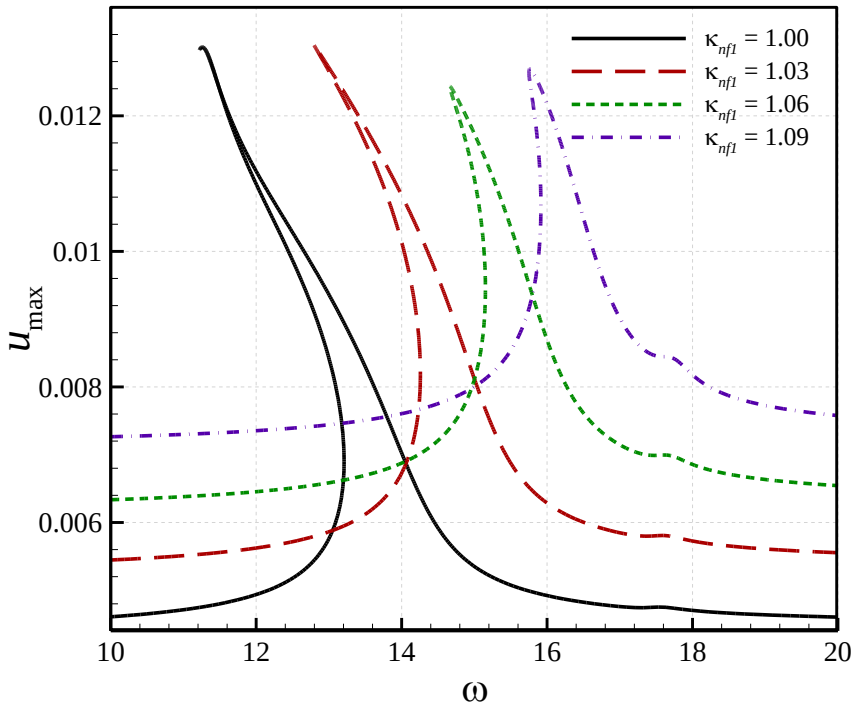

Fig. 12. Effects of κ_{nf1} on supercritical amplitude-frequency diagrams of the nanofluid-conveying nanoscale tube; (a) w_{max} at x=0.5; (b) u_{max} at x=0.657; U=6.5 and F_1=2.0.